JACS
JOURNAL OF THE AMERICAN CHEMICAL SOCIETY
pubs.acs.org/JACS
Article

Regulating the Assembly of γ-Cyclodextrin Host and Polyoxometalate-Based Guests toward Light-Responsive Hybrid Rotaxanes

Wu-Ji Chen,[§] Chun-Yan Liu,[§] Yun-Jing Mu, Yi-An Yin, Chang-Gen Lin,* De-Liang Long,* Leroy Cronin,* and Yu-Fei Song*

Cite This: J. Am. Chem. Soc. 2025, 147, 28903−28911

ABSTRACT: The rational design of hybrid organic−inorganic rotaxanes is crucial for advancing molecular machines and functional nanomaterials, yet the integration of metal-oxo clusters into interlocked systems remains challenging. Herein, we present a precision synthesis strategy for hybrid rotaxanes combining γ-cyclodextrin (γ-CD) hosts with Anderson-type polyoxometalate (POM)-based guests. This approach utilizes covalent POM modification coupled with strategically anchored organic functionalities to control supramolecular assembly, enabling the construction of *pseudo*-[2]-, [3]-, and [4]rotaxanes with controlled structural variations. Significantly, we achieved the first single-crystal examples of supramolecular *pseudo*-[4]rotaxanes featuring γ-CD dimers threaded by two organo-POM units. A key breakthrough was achieved through light-induced single-crystal-to-single-crystal transformation of these *pseudo*-[4]rotaxanes, producing hybrid [3]rotaxanes containing uniquely arranged *anti*-head-to-tail anthracene dimers—the first reported photoresponsive architecture of this type. These structural transformations demonstrate the dynamic, stimuli-responsive character of these hybrid systems. This work establishes a new paradigm for the precision engineering of rotaxanes using organo-POM building blocks, revealing their remarkable potential for creating smart materials with programmable structural changes. The successful integration of covalent modification, supramolecular templating, and photoresponsive components provides a powerful platform for developing next-generation multifunctional molecular machines and adaptive nanomaterials with precisely controlled properties.

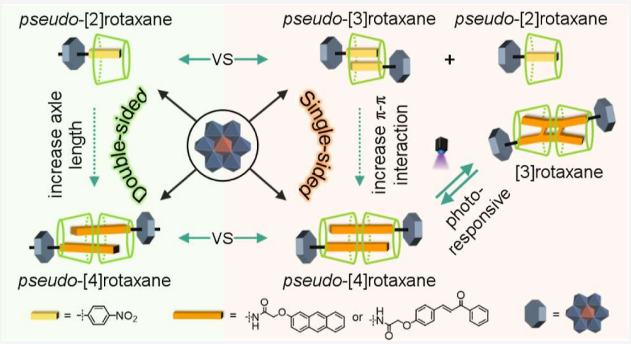

INTRODUCTION

Rotaxanes, a key subclass of mechanically interlocked molecules (MIMs),[1] consist of macrocyclic "wheels" threaded onto dumbbell-shaped "axles" capped with sterically bulky "stoppers" that prevent dethreading.[2] The [*n*]rotaxane nomenclature indicates a system of *n* interlocked components, while *pseudo*-rotaxanes represent their dynamic, stopper-lacking supramolecular analogues. These architectures have found widespread applications in catalysis,[3] molecular machines,[4] room-temperature phosphorescence,[5] and smart materials[6] due to their unique interlocked structures and stimuli-responsive behavior. A landmark achievement in this field is the γ-cyclodextrin (γ-CD)-templated enantioselective photodimerization of anthracene derivatives, which achieved up to 32% enantiomeric excess (ee) for the *syn*-head-to-tail configuration (Figure 1a).[7] Recent progress has focused on incorporating metal-coordination motifs as wheels to create hybrid rotaxanes, enabling novel functionalities in qubits, sensing, and nonlinear optical materials.[8−14] Despite significant advances in the rational design of macrocyclic wheels and axles in MIMs, the functional role of stoppers remains poorly understood, particularly their impact on solution-phase dynamics and solid-state structural organizations.

We therefore identified polyoxometalates (POMs)—discrete anionic metal-oxo clusters of early transition metals in their highest oxidation states[15−24]—as ideal inorganic stoppers for hybrid (*pseudo*-)rotaxane construction. POMs offer two key advantages: (i) their capacity for site-specific covalent functionalization enables rational design of hybrid architectures with programmable functionality, and (ii) their well-defined steric bulk provides effective stopper performance.[25−29] Previous works have demonstrated that organo-POM hybrids can be incorporated into rotaxane systems by utilizing their organic moieties as threading axles while employing the

Received: April 16, 2025
Revised: June 11, 2025
Accepted: July 23, 2025
Published: July 29, 2025

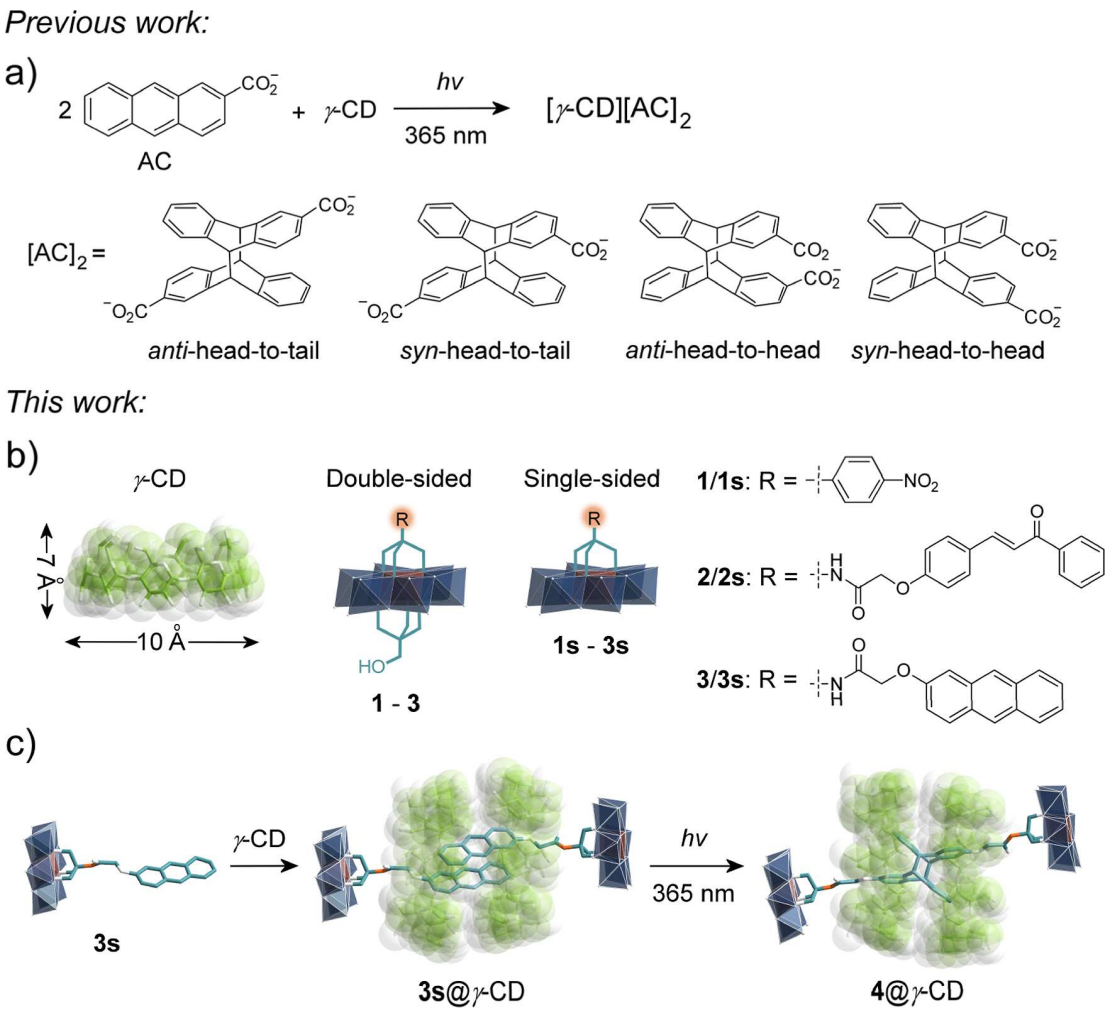

Figure 1. Schematic representation of (a) the photodimerization in MIMs formed by 2-anthracenecarboxylates and γ-CDs,[7] (b) the structures of γ-CD and asymmetric Anderson-type POM {$AlMo_6O_{24}$} hybrids, and (c) the *pseudo*-[4]rotaxane and photodimerized [3]rotaxane formed by POM hybrid **3s** and γ-CD. Color code: {MoO_6}, dark blue octahedron; {AlO_6}, brown octahedron; C, green in γ-CD and teal in POM hybrids; N, orange; and O, white.

inorganic clusters as steric barriers, with macrocyclic hosts like CDs serving as effective templates.[30−34]

The supramolecular recognition between organo-POMs and CDs occurs through hydrophobic guest−host interactions, fundamentally differing from the chaotropic interactions that drive unmodified POM-CD complexation (where POM's low charge density disrupts water structure).[35−48] This distinction led us to hypothesize that two key variables could synergistically control assembly thermodynamics and topology: (i) the covalent modification patterns of the POM cluster and (ii) the chemical nature of anchored organic units. By systematically tuning these parameters, we predicted precise control over POM stoppers' steric and recognition properties.

We investigated how site-specific covalent modification of Al-Anderson-type POMs {$AlMo_6O_{24}$}[49−51] dictates their recognition with γ-CDs (Figure 1b). Through comparative studies of double-sided versus single-sided asymmetric functionalization, we elucidated the distinct roles of steric effects and hydrogen-bonding interactions (mediated by free μ_3-O sites) in directing assembly pathways. Incorporating photoresponsive chalcone and anthracene derivatives enabled light-modulated supramolecular behavior. This strategy produced a series of well-defined POM-CD complexes, including *pseudo*-[2], [3], and [4]rotaxanes, all characterized by single-crystal X-ray diffraction. Our most significant achievement was the photoinduced single-crystal-to-single-crystal transformation of a *pseudo*-[4]rotaxane to a [3]rotaxane via anthracene dimerization under mild irradiation (Figure 1c). Our work establishes two landmark advances: (i) the first *pseudo*-[4]rotaxanes with γ-CD dimers threaded by two organo-POM axles; (ii) the first [3]rotaxane system containing pure *anti*-head-to-tail anthracene dimers—a configuration inaccessible through conventional synthesis.

RESULTS AND DISCUSSION

In our previous work, we reported the assembly of symmetrically functionalized Anderson hybrids with γ-CD, which characterized a poly-*pseudo*-rotaxane structure with two nitrobenzene units partially encapsulated in γ-CD cavities.[34] Here, using the double-sided asymmetric **1** (Figure 1b), we anticipated a *pseudo*-[3]rotaxane with a 2:1 (**1**:γ-CD) stoichiometry. Surprisingly, crystallization—even with excess γ-CD—yielded instead a 1:1 *pseudo*-[2]rotaxane, **1**@γ-CD, as unequivocally demonstrated by single-crystal X-ray diffraction (Figure 2a). The structure reveals close contacts between

https://doi.org/10.1021/jacs.5c06495
J. Am. Chem. Soc. 2025, 147, 28903−28911

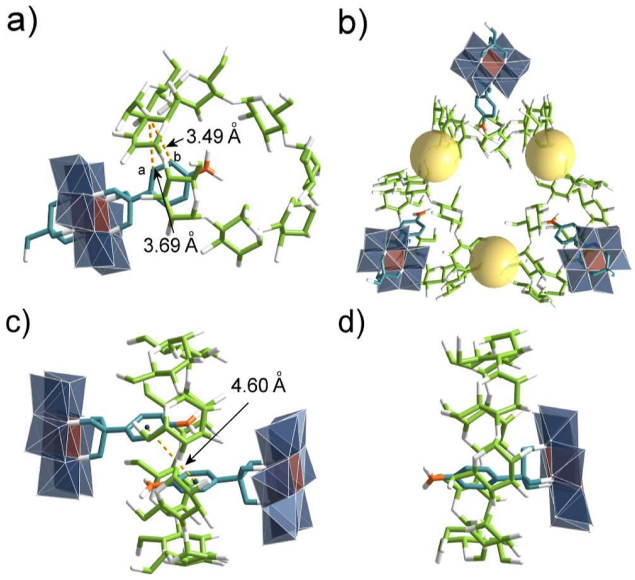

Figure 2. (a) The single-crystal structure of complex **1**@γ-CD, (b) the triangle oligomer of complex **1**@γ-CD linked by K^+ ions, and (c) the *pseudo*-[3]rotaxane structure and (d) the *pseudo*-[2]rotaxane in complex **1s**@γ-CD. Color code: {MoO_6}, dark blue octahedron; {AlO_6}, brown octahedron; C, green in γ-CD and teal in **1**; N, orange; O, white; and K, yellow sphere.

protons H_a/H_b of **1** and γ-CD's bridging oxygen atoms. The **1**@γ-CD assembly was further confirmed by ^{1}H NMR, 2D nuclear Overhauser effect spectroscopy (NOESY), electrospray ionization time-of-flight mass spectroscopy (ESI-TOF-MS), and isothermal titration calorimetry (ITC) (Figures S11–S15). Notably, in the crystal lattice, potassium ions bridge **1**@γ-CD units into triangular oligomers (Figure 2b).

Slow evaporation of an aqueous solution containing near-equimolar amounts of single-sided hybrid **1s** and γ-CD yielded X-ray quality crystals of **1s**@γ-CD. Unlike the **1**@γ-CD complex, the **1s**@γ-CD contains both *pseudo*-[3]rotaxane and *pseudo*-[2]rotaxane species (Figure 2c,d). In the *pseudo*-[3]rotaxane, two nitrobenzene units are deeply inserted into the γ-CD cavity (separation: 4.60 Å), significantly closer than the 6.22 Å distance observed in our previously reported symmetric system.[34] The *pseudo*-[2]rotaxane shows complete nitrobenzene inclusion, evidenced by strong NOESY correlations between H_a/H_b of **1s** and γ-CD's H_5/H_6 protons (Figures S18, S19). The asymmetric unit contains two *pseudo*-[3]rotaxanes, one *pseudo*-[2]rotaxane, and one free γ-CD, yielding an overall 5:4 (**1s**:γ-CD) stoichiometry (Figure S20).

This distinct assembly behavior stems from **1s**'s accessible μ_3-O sites, which form strong hydrogen bonding with γ-CD hydroxyl groups (Figure S20). In contrast, double-sided **1** lacks these interactions. The effect of hydrogen bonding has been confirmed by ^{27}Al NMR, where **1s**@γ-CD exhibited a clear upfield shift ($\Delta\delta$ = −0.27 ppm) when compared with single-sided **1s** (Figure S22), while a negligible shift was observed in the case of **1**@γ-CD (Figure S21). ESI-TOF-MS confirmed both *pseudo*-[2] and [3]rotaxane species in **1s**@γ-CD (Figure S23), while ITC measurements ($K = 7.36 \times 10^3$ M^{-1}) verified the 5:4 stoichiometry of **1s**@γ-CD and revealed twice the binding affinity of **1**@γ-CD (Figure S24), consistent with preferential *pseudo*-[3]rotaxane formation in **1s**@γ-CD (Table S1).

Encouraged by these results, we next examined γ-CD complexation with chalcone-functionalized hybrids **2** and **2s**, anticipating UV-triggered [2 + 2] cycloaddition on the π-conjugated chalcone groups.[52] Herein, we focus on a discussion of the details for **2**. Contrary to our hypothesis of 2:1 *pseudo*-[3]rotaxane formation, multiple lines of evidence indicated 1:1 complexation of **2** with γ-CD in solution: (i) ^{1}H NMR showed significant upfield shifts of the chalcone protons upon γ-CD addition, particularly for H_d and H_c ($\Delta\delta$ = −0.66 and −0.44, respectively) of the α, β-unsaturated carbonyl group and H_i ($\Delta\delta$ = −0.57) (Figure 3a, S27), suggesting there may be a deep threading of the chalcone moiety in γ-CD; (ii) the Job plot analysis (UV–vis at 340 nm) showed maximum complexation at 1:1 ratio (Figure 3b); and (iii) ITC confirmed 1:1 stoichiometry ($K = 1.38 \times 10^3$ M^{-1}) (Figure 3c and Table S1). While these results clearly demonstrate 1:1 complex formation, precise intermolecular interactions require further investigation.

Through slow evaporation of an aqueous solution containing **2** and 10 equiv of γ-CD, we obtained single crystals of the **2**@γ-CD complex. X-ray analysis revealed that **2**@γ-CD crystallizes in an orthorhombic system with a $P2_12_12_1$ space group, two asymmetric **2** and two γ-CDs, forming a *pseudo*-[4]rotaxane structure of 2:2 adduct in the asymmetric unit (Figure 4a). Based on the conformations of the oxy-acetamide groups, *i.e.*, the positions of the two oxygen atoms (highlighted in Figures 4a, S28), the two asymmetric **2** molecules can be classified into *Z*- and *E*-isomers. Notably, the chalcone moieties of the isomers thread into a "head-to-head" γ-CD dimer. While previous reports have described *pseudo*-[3]-rotaxanes with α-CD dimers[53,54] or β-CD dimers,[55,56] **2**@γ-CD represents the first case of *pseudo*-[4]rotaxane structure featuring two guest molecules threaded through a γ-CD pair. The observed 1:1 molar ratio in complex **2**@γ-CD agrees perfectly with our titration experiments.

ESI-TOF-MS analysis of **2**@γ-CD (Figures 3d, S29) revealed two major fragments: a 1:1 adduct of **2** and γ-CD, and a 1:2 adduct. The absence of a 2:2 adduct likely results from fragmentation during ionization. The presence of the 1:2 adduct, such as $\{\mathbf{2}@(\gamma\text{-CD})_2\}^{3-}$ species, suggests these complexes may exist transiently in solution, though the thermodynamically favored 2:2 adduct crystallizes in the solid state exclusively, as confirmed by crystallization experiments across various stoichiometric ratios (1:1 to 1:10).

The *Z*- and *E*-isomers in **2**@γ-CD exhibit close through-space contacts, with $C_b\cdots C_{d*}$ and $C_a\cdots C_{e*}$ distances measured at 3.45 and 3.81 Å, respectively (Figure 4b). These interactions were corroborated by 2D NOESY, showing spatial correlations between H_b-H_d and H_a-H_e (Figure 3e). Additional interactions between γ-CD and the two isomers were observed (Figure 4c,d), including close C_i-C_5 contacts (3.83 Å for *Z*-isomer and 3.72 Å for *E*-isomer) that explain the upfield shift of H_i in ^{1}H NMR (Figure 3a). Despite these proximities, the α, β-unsaturated carbonyl groups remain separated by 4.46–5.36 Å—beyond the 4.2 Å Schmidt distance[57] for [2 + 2] photocycloaddition (Figure S28). Parallel studies with single-sided **2s** yielded similar inclusion complexes (Figures S31–S35), though we were unable to obtain X-ray quality crystals of **2s**@γ-CD.

To further validate the formation of *pseudo*-[4]rotaxanes between γ-CD and asymmetric Anderson hybrids, while also pursuing the targeted synthesis of [3]rotaxanes through photoinduced single-crystal-to-single-crystal transformation,

https://doi.org/10.1021/jacs.5c06495
J. Am. Chem. Soc. 2025, 147, 28903–28911

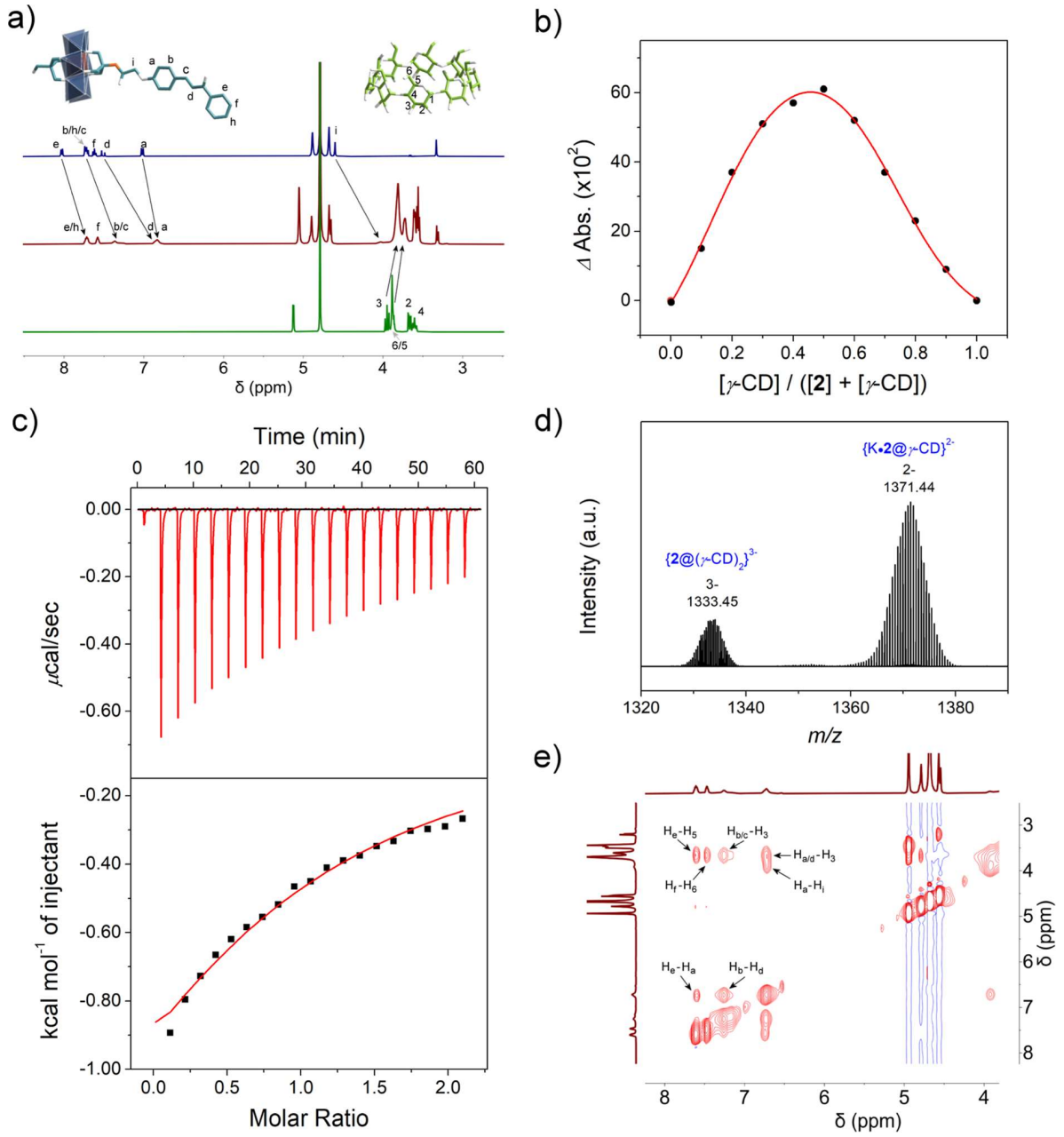

Figure 3. (a) The ^{1}H NMR spectrum of **2** (top), **2**@γ-CD (middle), and γ-CD (bottom) in D_2O; (b) the Job plot of the UV−vis absorbance changes at 340 nm showing the molar ratio of γ-CD and **2** upon complexation; (c) the ITC thermogram (top) and isotherm (bottom) of **2**@γ-CD, dots and lines correspond to experimental and theoretical heat values, respectively; (d) the ESI-TOF-MS of **2**@γ-CD at m/z = 1371.44 and 1333.45; and e) the 2D NOESY ^{1}H NMR spectrum of **2**@γ-CD in D_2O.

we focused on the asymmetric hybrid **3**, which contains a more π-conjugated anthracene moiety. The flat and π-conjugated anthracene was strategically incorporated to enhance the $\pi-\pi$ interactions, thereby facilitating the reduction of intermolecular distances required to meet the Schmidt's criteria for photodimerization. Using ^{1}H NMR titration to monitor the complexation between **3** and γ-CD, we observed significantly more complex assembly behavior compared to the analogous system with hybrid **2**.

As shown in Figure 5, titration of γ-CD into a 6 mM solution of **3** induced characteristic upfield shifts of anthracene proton signals, accompanied by significant peak broadening indicative of rapid host−guest exchange dynamics. The complexation process has three distinct stages. The first stage is the initial binding (0−0.5 equiv of γ-CD), where progressive upfield shifts are observed for all anthracene protons except H_g and H_f. This is consistent with the partial inclusion of the anthracene moiety within γ-CD cavities. The second stage is the structural reorganization (0.5−1 equiv of γ-CD), where chemical shift changes are plateaued and there is emergence of signal splitting for key protons: H_f bifurcated into downfield (f') and upfield components, H_c developed new upfield resonance (c'), suggesting an equilibrium shift between multiple complexation modes. The third stage is the secondary complex formation (>1 equiv of γ-CD), where broad peaks (i', d') appear at chemical shifts matching free **3**, indicating the formation of

https://doi.org/10.1021/jacs.5c06495
J. Am. Chem. Soc. 2025, 147, 28903−28911

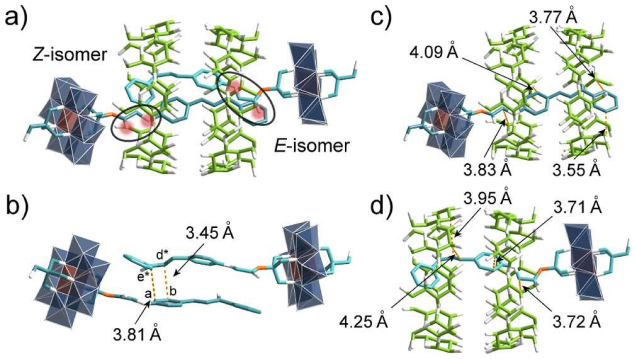

Figure 4. (a) The single-crystal structure of complex **2**@γ-CD (the *Z*- and *E*-isomers are labeled), (b) the intermolecular distances (in yellow dotted lines) between the chalcone molecules in complex **2**@γ-CD, and (c and d) the intermolecular distances between γ-CD and the *Z*- and *E*-isomers of **2**. Color code: the same as that in Figure 2, and carbon in *E*-isomer is represented in cyan.

new species in γ-CD-rich environment. This multistage evolution of NMR signatures reveals complex, concentration-dependent equilibria between distinct host−guest assemblies, with the observed splitting patterns being particularly suggestive of structural reorganization at intermediate γ-CD concentrations.

Along with the proton shifting and splitting in the aromatic region, the inner γ-CD protons also experienced similar changes. In the first stage, H_3, H_5, and H_6 proton signals of γ-CD all shift upfield relative to free γ-CD in D_2O. During the second stage, these protons shifted downfield, while H_6 and H_5 underwent splitting, generating new resonances at 3.90 ppm (designated 6′/5′, Figure 5). The intensity of these split peaks increased before diminishing as additional γ-CD was introduced (1−6 equiv). In the last stage, with excess γ-CD, all H_3, H_5, and H_6 proton signals returned to their original chemical shifts, matching those of uncomplexed γ-CD.

To better understand the complexation process during titration, we attempted to crystallize assembly intermediates by preparing aqueous mixtures of **3** and γ-CD at 3:1, 1:1, and 1:3 molar ratios. Despite varying the stoichiometry, all crystallization attempts yielded single crystals of 2:2 adducts, mirroring the behavior observed for **2**@γ-CD. X-ray crystallography revealed that **3**@γ-CD adopts a *pseudo*-[4]rotaxane structure, with both the *Z*- and *E*-isomers of **3** threading through a γ-CD dimer (Figure 6a). The anthracene moieties in both isomers display strong intermolecular interactions with the γ-CD dimer (Figure 6b,c), while also exhibiting close contacts between themselves. As denoted in Figure 6e, key intermolecular distances include $C_c\cdots C_{d*}$ (3.55 Å) and $C_{c*}\cdots C_d$ (3.54 Å), with C_{f*} of the *E*-isomer positioned

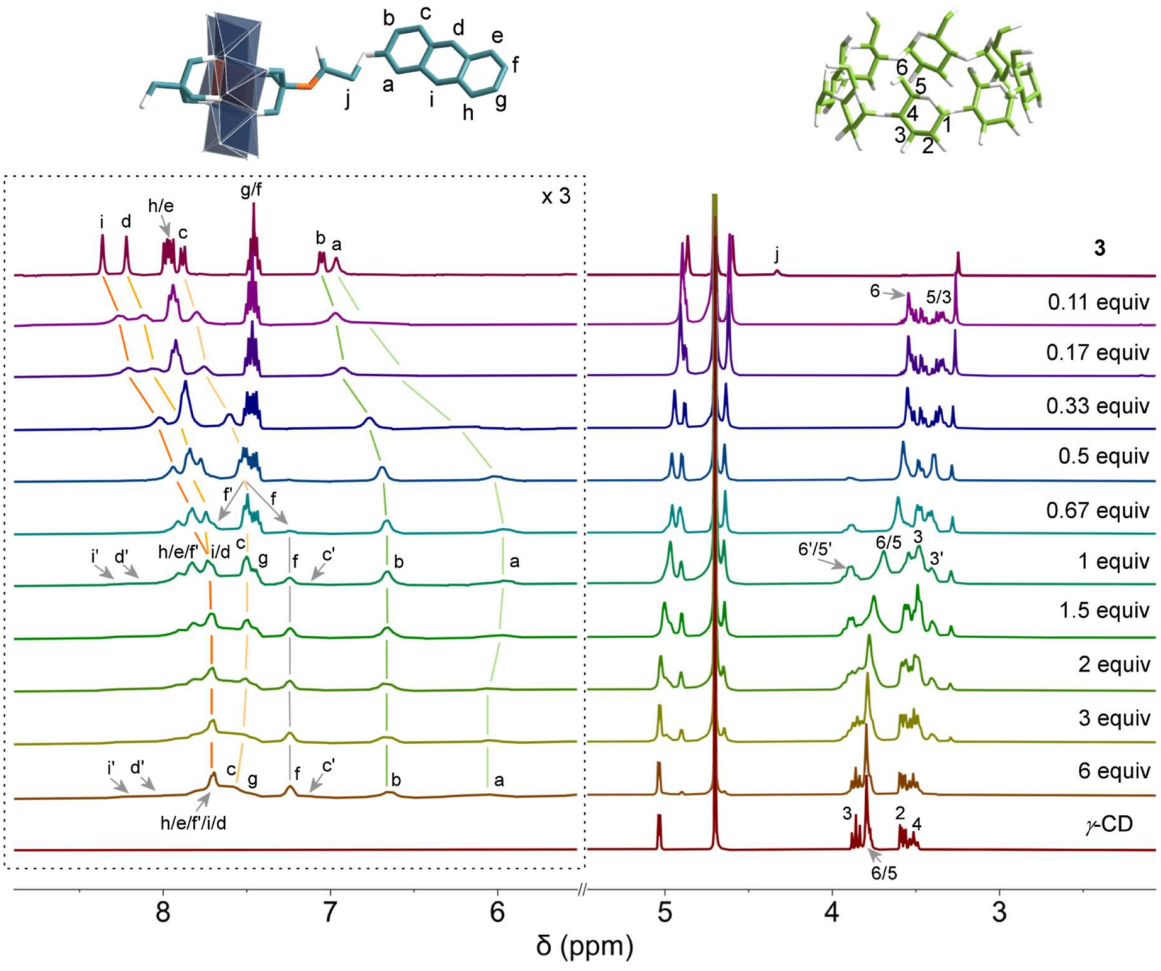

Figure 5. ^{1}H NMR titration of the supramolecular assembly of γ-CD and **3** upon successive addition of γ-CD into **3** in D_2O (c = 6 mmol/L). The equivalent amounts of γ-CD to **3** are labeled.

https://doi.org/10.1021/jacs.5c06495
J. Am. Chem. Soc. 2025, 147, 28903−28911

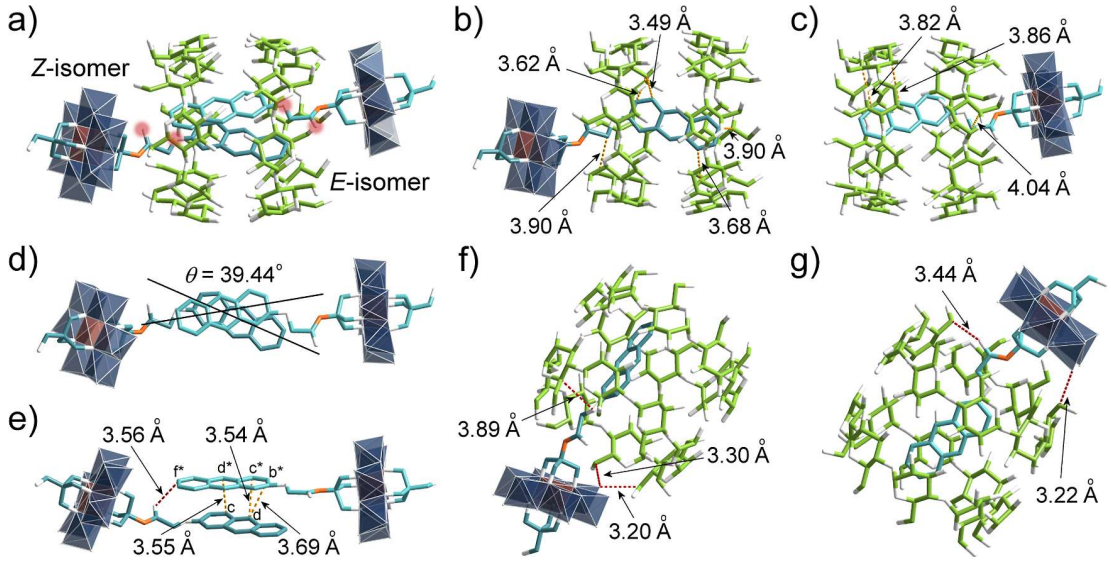

Figure 6. (a) The single-crystal structure of complex **3**@γ-CD, (b) and (c) the intermolecular distances (in yellow dotted lines) between γ-CD and the *Z*- and *E*-isomers of **3**, (d) the twisted angle and (e) the intermolecular distances between the anthracene molecules in complex **3**@γ-CD, and (f and g) the close distances (in red dotted lines) between C_5/C_6 of γ-CDs and the oxygen atoms in **3**. Color code: the same as in Figure 2, and carbon in *E*-isomer is represented in cyan.

near the *Z*-isomer's carbonyl group (d = 3.56 Å). These structural features explain the H_c and H_f splitting observed during the second stage of NMR titration, confirming the presence of 2:2 adducts in solution. Additional short contacts between the C_5/C_6 atoms of γ-CDs and the oxygen atoms of **3** (Figure 6f,g) account for the observed H_5/H_6 splitting in the low-field NMR region. ITC (Figure S41) and UV−vis titration (Figure S42) further confirmed the 1:1 stoichiometry of complex **3**@γ-CD in solution. While previous studies have reported anthracene anchoring on Mn-Anderson clusters[58] and proposed 2:1 anthracene-γ-CD adducts,[59] our work provides definitive structural evidence for 2:2 adduct formation, likely attributable to distinct structural features of the Anderson hybrids. Although the anthracene spatial distances are at 9 ($C_d\cdots C_{d^*}$) and 10 ($C_i\cdots C_{i^*}$) positions (Figure S43) satisfy Schmidt's criterion, no dimerization of **3**@γ-CD was observed, presumably due to the big twist angle (θ = 39.44°) between anthracene moieties (Figure 6d).

Based on combined analyses of the ^{1}H NMR titration and X-ray data, we proposed the following assembly pathway: initial addition of γ-CD into the solution of **3** generates 2:1 adducts, reaching maximum formation at 0.5 equiv of γ-CD. As the γ-CD ratio increases to 1 equiv, these 2:1 adducts gradually convert to 2:2 complexes. Further γ-CD addition (beyond 1 equiv) promotes formation of new 1:2 species (Figure S38a). 2D NOESY studies at varying molar ratios support this mechanism. For the 3:1 mixture (excess **3**), observed spatial correlations between H_e-H_a and H_i-H_c of anthracene units indicate a significant twisting angle between π-conjugated moieties (Figure S38b). Additional through-space correlations between anthracene ($H_i/H_h/H_e/H_c$) and γ-CD (H_3/H_5) protons closely resemble those reported for 2:1 adducts of 2-anthracenecarboxylates and γ-CDs.[7] The 1:1 mixture shows distinct behavior, with only H_d-$H_{c'}$ spatial correlation between threaded anthracenes (Figure S39), matching the X-ray structure (Figure 6b,c). In the 1:3 mixture (excess γ-CD), the disappearance of intermolecular correlations and appearance of solely *J*3-couplings suggest the inclusion of one anthracene molecule in the cavities of the γ-CD dimer (Figure S38c). ESI-TOF-MS analysis of **3**@γ-CD (Figure S40) further confirms solution-phase equilibria, showing a dominant 1:1 adduct, secondary 1:2 species (similar to the case of **2**@γ-CD), minor 2:1 adducts such as $\{K_3\cdot(\mathbf{3})_2@\gamma\text{-CD}\}^{3-}$ and $\{K_2\cdot(\mathbf{3})_2@\gamma\text{-CD}\}^{4-}$, and trace 2:2 fragments $K_3\cdot(\mathbf{3})_2@(\gamma\text{-CD})_2\}^{3-}$ (Table S2).

We subsequently examined single-sided **3s**, which exhibited nearly identical solution-phase assembly behavior with γ-CD as observed for **3**, as confirmed by multiple characterization techniques (Figures S45−S49). Single crystals of **3s**@γ-CD were obtained through slow evaporation of an aqueous solution containing near-equimolar amounts of **3s** and γ-CD. Unlike the structures of **2**@γ-CD and **3**@γ-CD that contain both *Z*- and *E*-isomers, X-ray diffractions revealed that **3s**@γ-CD crystallizes exclusively with the *Z*-isomer in a 2:2 *pseudo*-[4]rotaxane arrangement (Figure 7a). This structural distinction likely arises from strong intermolecular hydrogen

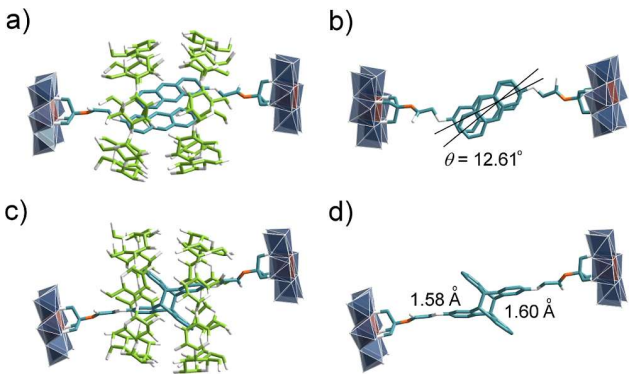

Figure 7. (a) The single-crystal structure of complex **3s**@γ-CD, (b) the twisted angle between the anthracene molecules in complex **3s**@γ-CD, (c) the single-crystal structure of complex **4**@γ-CD, and (d) the bond distances between 9 and 10 positions of the anthracene-dimer in complex **4**@γ-CD. Color code: the same as in Figure 2.

https://doi.org/10.1021/jacs.5c06495
J. Am. Chem. Soc. 2025, 147, 28903−28911

bonding between γ-CD and the μ_3-O sites of single-sided **3s**, as evidenced by short O···O contact distances in the crystal packing (Figure S50). The structure also shows close anthracene-γ-CD interactions (Figure S51), consistent with 2D NOESY observations (Figure S46). Importantly, the twist angle between anthracene moieties decreases significantly to 12.61° (Figure 7b), while maintaining favorable $C_9\cdots C_{9*}$ (3.67 Å) and $C_{10}\cdots C_{10*}$ (3.72 Å) distances (Figure S52)—parameters that satisfy both geometric and electronic requirements for successful [4 + 4] photodimerization via single-crystal-to-single-crystal transformation.

To verify the photodimerization, single crystals of **3s**@γ-CD were coated with Paratone oil and irradiated with 365 nm UV light. Following extensive optimization, high-quality single crystals of **4**@γ-CD were obtained after 8 h of irradiation (Figure S59). X-ray analysis revealed **4**@γ-CD to be a [3]rotaxane, representing—to our knowledge—the first structurally characterized single-crystal rotaxanes incorporating an anthracene dimer within γ-CDs (Figure 7c). The unit cell of **4**@γ-CD slightly expanded (orthorhombic, a = 24.6852(8), b = 27.9765(9), c = 39.4067(13), V = 27214.5(15) Å^3), compared with that of **3s**@γ-CD (orthorhombic, a = 24.7051(5), b = 27.7438(6), c = 38.6548(10), V = 26494.5(10) Å^3) (Table S3). The cell volume increased by nearly 3% after photodimerization. The bond distances (Figure 7d) between the 9 and 10 positions of anthracene-dimer match those reported for polymerized anthracene 2D polymers.[60] In a recent report by Shen and Stoddart et al.,[61] 1-anthracene-carboxylates were incorporated into γ-CD-MOFs for the selective formation of *anti*-head-to-head anthracene dimers in *ca.* 80% *ee* yield. However, crystal structures of such *anti*-head-to-head dimers have not been reported. Here in our system, the constrained geometry of **3s** enforces an exclusive *anti*-head-to-tail alignment in both **3s**@γ-CD and its photoproduct **4**@γ-CD.

The photodimerization was further characterized by ^{1}H NMR and 2D NOESY, despite the significantly reduced water solubility of **4**@γ-CD. The ^{1}H NMR spectrum (Figure S54) revealed dramatic changes for H_i and H_d protons, which shifted upfield by $\Delta\delta$ = −3.28 and −3.43 ppm, respectively, moving from the aromatic to aliphatic region. The 2D NOESY spectrum of **4**@γ-CD showed distinct J3-couplings between H_i/H_d and their neighboring protons (Figure S55), contrasting sharply with the through-space correlations (H_e-H_a and H_h-H_b) observed for **3s**@γ-CD (Figure S46). Solid-state UV−vis spectroscopy confirmed the photodimerization through complete disappearance of the characteristic anthracene absorption at 255 nm and the weak fine absorptions in the range 330−380 nm (Figure S56). Fluorescence studies provided additional evidence with the broad emission band (400−500 nm) of **3s**@γ-CD being completely absent in **4**@γ-CD (Figure S57).

The anthracene dimerization proved to be thermally reversible. Heating bulk samples of **4**@γ-CD at 150 °C for 2 h (Figure S60) regenerated the monomeric form, as evidenced by (i) disappearance of the aliphatic H_i and H_d signals and (ii) restoration of proton chemical shifts matching those in original **3s**@γ-CD (Figure S61). Recrystallization of the thermally treated material from water successfully regenerated **3s**@γ-CD single crystals, completing the reversible cycle.

CONCLUSIONS

In summary, we successfully demonstrated the supramolecular assembly of γ-CDs with asymmetrically functionalized Anderson-type POMs to construct novel *pseudo*-rotaxane architectures. The covalent modification pattern of Anderson POMs proved to be an effective strategy for designing new POM-CD complexes, enabling the fabrication of a series of organic−inorganic hybrid rotaxanes, including *pseudo*-[2]-, [3]-, and [4]rotaxane structures. Notably, the *pseudo*-[4]-rotaxanes represent the first single-crystal examples of γ-CD dimers threaded by two organo-POMs. Through photoinduced single-crystal-to-single-crystal transformation, we achieved conversion of these *pseudo*-[4]rotaxanes to hybrid [3]rotaxanes featuring: (i) a γ-CD dimer as the wheel, (ii) a photopolymerized anthracene dimer as the axle, and (iii) two Anderson POMs as stoppers. This system also provides the first single-crystal structural characterization of an *anti*-head-to-tail anthracene dimer arrangement within a rotaxane framework. Current efforts in our laboratory are focused on extending this approach to construct 2D/3D MIM frameworks using organo-POM building blocks with the goal of developing functional materials for chiral adsorption, catalysis, and stimuli-responsive applications.

ASSOCIATED CONTENT

Supporting Information

The Supporting Information is available free of charge at https://pubs.acs.org/doi/10.1021/jacs.5c06495.

Synthetic procedures, NMR, ITC, crystallography, and other materials (PDF)

Accession Codes

Accession Codes CCDC nos. 2409910−2409916 contain the supplementary crystallographic data for this paper. These data are provided free of charge by the joint Cambridge Crystallographic Data Centre and Fachinformationszentrum Karlsruhe (http://www.ccdc.cam.ac.uk/structures) Access Structures service.

AUTHOR INFORMATION

Corresponding Authors

Chang-Gen Lin − *State Key Laboratory of Chemical Resource Engineering, Beijing University of Chemical Technology, Beijing 100029, P. R. China;* orcid.org/0000-0003-4541-4509; Email: linchg@mail.buct.edu.cn

De-Liang Long − *School of Chemistry, The University of Glasgow, Glasgow G11 6EW, U.K.;* orcid.org/0000-0003-3241-2379; Email: deliang.long@glasgow.ac.uk

Leroy Cronin − *School of Chemistry, The University of Glasgow, Glasgow G11 6EW, U.K.;* orcid.org/0000-0001-8035-5757; Email: lee.cronin@glasgow.ac.uk

Yu-Fei Song − *State Key Laboratory of Chemical Resource Engineering, Beijing University of Chemical Technology, Beijing 100029, P. R. China;* orcid.org/0000-0003-1309-0626; Email: songyf@mail.buct.edu.cn

Authors

Wu-Ji Chen − *State Key Laboratory of Chemical Resource Engineering, Beijing University of Chemical Technology, Beijing 100029, P. R. China*

Chun-Yan Liu − *State Key Laboratory of Chemical Resource Engineering, Beijing University of Chemical Technology, Beijing 100029, P. R. China*

Yun-Jing Mu − *State Key Laboratory of Chemical Resource Engineering, Beijing University of Chemical Technology, Beijing 100029, P. R. China*

Yi-An Yin − *State Key Laboratory of Chemical Resource Engineering, Beijing University of Chemical Technology, Beijing 100029, P. R. China*

Complete contact information is available at: https://pubs.acs.org/10.1021/jacs.5c06495

Author Contributions

[§]W.-J. C. and C.-Y. L. contributed equally to this work.

Notes

The authors declare no competing financial interest.

■ ACKNOWLEDGMENTS

This research was supported by the National Natural Science Foundation of China (22288102, 22178019, 22208013, 22378012), the Fundamental Research Funds for the Central Universities (XK1802-6, XK1803-05, XK1902), and the State Key Laboratory of Chemical Resource Engineering of Beijing University of Chemical Technology (CRE-24-C005). We also gratefully acknowledge the financial support by the EPSRC (nos. EP/L023652/1, EP/R009902/1, EP/R020914/1, EP/R01308X/1, EP/S017046/1, EP/S019472/1, EP/V048341/1), the European Research Council (Project 670467 SMART-POM), and the University of Glasgow.

■ REFERENCES

(1) Stoddart, J. F. Mechanically interlocked molecules (MIMs) − molecular shuttles, switches, and machines (Nobel Lecture). *Angew. Chem., Int. Ed.* **2017**, *56*, 11094−11125.

(2) Xue, M.; Yang, Y.; Chi, X.; Yan, X.; Huang, F. Development of pseudorotaxanes and rotaxanes: from synthesis to stimuli-responsive motions to applications. *Chem. Rev.* **2015**, *115*, 7398−7501.

(3) Heard, A. W.; Suárez, J. M.; Goldup, S. M. Controlling catalyst activity, chemoselectivity and stereoselectivity with the mechanical bond. *Nat. Rev. Chem.* **2022**, *6*, 182−193.

(4) Seale, J. S. W.; Feng, Y.; Feng, L.; Astumian, R. D.; Stoddart, J. F. Polyrotaxanes and the pump paradigm. *Chem. Soc. Rev.* **2022**, *51*, 8450−8475.

(5) Zhang, T.; Ma, X.; Wu, H.; Zhu, L.; Zhao, Y.; Tian, H. Molecular engineering for metal-free amorphous materials with room-temperature phosphorescence. *Angew. Chem., Int. Ed.* **2020**, *59*, 11206−11216.

(6) Nakahata, M.; Takashima, Y.; Hashidzume, A.; Harada, A. Redox-generated mechanical motion of a supramolecular polymeric actuator based on host-guest interactions. *Angew. Chem., Int. Ed.* **2013**, *52*, 5731−5735.

(7) Nakamura, A.; Inoue, Y. Supramolecular catalysis of the enantiodifferentiating [4 + 4] photocyclodimerization of 2-anthracenecarboxylate by γ-cyclodextrin. *J. Am. Chem. Soc.* **2003**, *125*, 966−972.

(8) Altmann, P. J.; Pöthig, A. A pH-dependent, mechanically interlocked switch: organometallic [2]rotaxane vs. organic [3]-rotaxane. *Angew. Chem., Int. Ed.* **2017**, *56*, 15733−15736.

(9) Altmann, P. J.; Pöthig, A. Pillarplexes: a metal-organic class of supramolecular hosts. *J. Am. Chem. Soc.* **2016**, *138*, 13171−13174.

(10) Liu, Y.-J.; Zheng, C.; Xiao, H.; Wang, Z.; Zhang, C.-Y.; Wang, S.-T.; Fang, W.-H.; Zhang, J. Designed synthesis of an aluminum molecular ring based rotaxane and polyrotaxane. *Angew Chem Int Ed Engl* **2024**, *136*, No. e202411576.

(11) Lee, C.-F.; Leigh, D. A.; Pritchard, R. G.; Schultz, D.; Teat, S. J.; Timco, G. A.; Winpenny, R. E. P. Hybrid organic-inorganic rotaxanes and molecular shuttles. *Nature* **2009**, *458*, 314−318.

(12) Lockyer, S. J.; Fielding, A. J.; Whitehead, G. F. S.; Timco, G. A.; Winpenny, R. E. P.; McInnes, E. J. L. Close Encounters of the Weak Kind: Investigations of Electron−Electron Interactions between Dissimilar Spins in Hybrid Rotaxanes. *J. Am. Chem. Soc.* **2019**, *141*, 14633−14642.

(13) Lockyer, S. J.; Nawaz, S.; Brookfield, A.; Fielding, A. J.; Vitorica-Yrezabal, I. J.; Timco, G. A.; Burton, N. A.; Bowen, A. M.; Winpenny, R. E. P.; McInnes, E. J. L. Conformational Flexibility of Hybrid [3]- and [4]-rotaxanes. *J. Am. Chem. Soc.* **2020**, *142*, 15941−15949.

(14) Fernandez, A.; Ferrando-Soria, J.; Pineda, E. M.; Tuna, F.; Vitorica-Yrezabal, I. J.; Knappke, C.; Ujma, J.; Muryn, C. A.; Timco, G. A.; Barran, P. E.; Ardavan, A.; Winpenny, R. E. P. Making hybrid [*n*]-rotaxanes as supramolecular arrays of molecular electron spin qubits. *Nat. Commun.* **2016**, *7*, 10240.

(15) Cronin, L.; Müller, A. From serendipity to design of polyoxometalates at the nanoscale, aesthetic beauty and applications. *Chem. Soc. Rev.* **2012**, *41*, 7333−7334.

(16) Stuckart, M.; Monakhov, K. Y. Polyoxometalates as components of supramolecular assemblies. *Chem. Sci.* **2019**, *10*, 4364−4376.

(17) Zhang, S.; Shi, W.; Wang, X. Locking volatile organic molecules by subnanometer inorganic nanowire-based organogels. *Science* **2022**, *377*, 100−104.

(18) Bonchio, M.; Syrgiannis, Z.; Burian, M.; Marino, N.; Pizzolato, E.; Dirian, K.; Rigodanza, F.; Volpato, G. A.; La Ganga, G.; Demitri, N.; Berardi, S.; Amenitsch, H.; Guldi, D. M.; Caramori, S.; Bignozzi, C. A.; Sartorel, A.; Prato, M. Hierarchical organization of perylene bisimides and polyoxometalates for photo-assisted water oxidation. *Nat. Chem.* **2019**, *11*, 146−153.

(19) Li, D.-H.; Zhang, X.-Y.; Lv, J.-Q.; Cai, P.-W.; Sun, Y.-Q.; Sun, C.; Zheng, S.-T. Photo-activating biomimetic polyoxomolybdate for boosting oxygen evolution in neutral electrolytes. *Angew. Chem., Int. Ed.* **2023**, *62*, No. e202312706.

(20) Amthor, S.; Knoll, S.; Heiland, M.; Zedler, L.; Li, C.; Nauroozi, D.; Tobaschus, W.; Mengele, A. K.; Anjass, M.; Schubert, U. S.; Dietzek-Ivanšić, B.; Rau, S.; Streb, C. A photosensitizer-polyoxometalate dyad that enables the decoupling of light and dark reactions for delayed on-demand solar hydrogen production. *Nat. Chem.* **2022**, *14*, 321−327.

(21) Hou, T.; Xu, W.; Pei, X.; Jiang, L.; Yaghi, O. M.; Persson, K. A. Ionic conduction mechanism and design of metal-organic framework based quasi-solid-state electrolytes. *J. Am. Chem. Soc.* **2022**, *144*, 13446−13450.

(22) Pakulski, D.; Gorczyński, A.; Brykczyńska, D.; Montes-García, V.; Czepa, W.; Janica, I.; Bielejewski, M.; Kubicki, M.; Patroniak, V.; Samorì, P.; Ciesielski, A. New Anderson-based polyoxometalate covalent organic frameworks as electrodes for energy storage boosted through keto-enol tautomerization. *Angew. Chem., Int. Ed.* **2023**, *62*, No. e202305239.

(23) Chang, Q.; Meng, X.; Ruan, W.; Feng, Y.; Li, R.; Zhu, J.; Ding, Y.; Lv, H.; Wang, W.; Chen, G.; Fang, X. Metal-organic cages with $\{SiW_9Ni_4\}$ polyoxotungstate nodes. *Angew. Chem., Int. Ed.* **2022**, *61*, No. e202117637.

(24) Lu, M.; Zhang, M.; Liu, J.; Yu, T.-Y.; Chang, J.-N.; Shang, L.-J.; Li, S.-L.; Lan, Y.-Q. Confining and highly dispersing single polyoxometalate clusters in covalent organic frameworks by covalent linkages for CO_2 photoreduction. *J. Am. Chem. Soc.* **2022**, *144*, 1861−1871.

(25) Song, Y.-F.; Tsunashima, R. Recent advances on polyoxometalate-based molecular and composite materials. *Chem. Soc. Rev.* **2012**, *41*, 7384−7402.

(26) Lin, C. G.; Fura, G. D.; Long, Y.; Xuan, W.; Song, Y.-F. Polyoxometalate-based supramolecular hydrogels constructed through host-guest interactions. *Inorg. Chem. Front.* **2017**, *4*, 789−794.

(27) Xia, Z.; Lin, C.-G.; Yang, Y.; Wang, Y.; Wu, Z.; Song, Y.-F.; Russell, T. P.; Shi, S. Polyoxometalate-surfactant assemblies: responsiveness to orthogonal stimuli. *Angew. Chem., Int. Ed.* **2022**, *61*, No. e202203741.

(28) Cameron, J. M.; Guillemot, G.; Galambos, T.; Amin, S. S.; Hampson, E.; Mall Haidaraly, K.; Newton, G. N.; Izzet, G. Supramolecular assemblies of organo-functionalised hybrid polyoxometalates: from functional building blocks to hierarchical nanomaterials. *Chem. Soc. Rev.* **2022**, *51*, 293−328.
(29) Anyushin, A. V.; Kondinski, A.; Parac-Vogt, T. N. Hybrid polyoxometalates as post-functionalization platforms: from fundamentals to emerging applications. *Chem. Soc. Rev.* **2020**, *49*, 382−432.
(30) Liu, C.-Y.; Mu, Y.-J.; Chen, W.-J.; Yin, Y.-A.; Lin, C.-G.; Miras, H. N.; Song, Y.-F. Modulating the supramolecular assembly of α-cyclodextrin and Anderson-type polyoxometalate through covalent modifications. *Chem.−Eur. J.* **2025**, *31*, No. e202403520.
(31) Yin, Y.-A.; Chen, W.-J.; Liu, C.-Y.; Zhang, M.-M.; Lin, C.-G.; Miras, H. M.; Song, Y.-F. Supramolecular assembly of covalently modified Anderson-type polyoxometalates and crown ethers towards *pseudo*-rotaxane structures. *Polyoxometalates* **2025**, *4*, 9140081.
(32) Izzet, G.; Ménand, M.; Matt, B.; Renaudineau, S.; Chamoreau, L.-M.; Sollogoub, M.; Proust, A. Cyclodextrin-induced auto-healing of hybrid polyoxometalates. *Angew. Chem., Int. Ed.* **2012**, *51*, 487−490.
(33) Bamba, I. F.; Falaise, C.; Marrot, J.; Atheba, P.; Gbassi, G.; Landy, D.; Shepard, W.; Haouas, M.; Cadot, E. Host-guest complexation between cyclodextrins and hybrid hexavanadates: what are the driving forces? *Chem.−Eur. J.* **2021**, *27*, 15516−15527.
(34) Yin, Y.-A.; Chen, W.-J.; Liu, C.-Y.; Zhang, M.-M.; Lin, C.-G.; Tsunashima, R.; Miras, H. N.; Song, Y.-F. Manipulating the supramolecular assembly of γ-cyclodextrin and Anderson polyoxometalate hybrids through variations in remote functionality. *Cell Rep. Phys. Sci.* **2024**, *5*, 102061.
(35) Assaf, K. I.; Nau, W. M. The chaotropic effect as an assembly motif in chemistry. *Angew. Chem., Int. Ed.* **2018**, *57*, 13968−13981.
(36) Yao, S.; Falaise, C.; Ivanov, A. A.; Leclerc, N.; Hohenschutz, M.; Haouas, M.; Landy, D.; Shestopalov, M. A.; Bauduin, P.; Cadot, E. Hofmeister effect in the Keggin-type polyoxotungstate series. *Inorg. Chem. Front.* **2021**, *8*, 12−25.
(37) Wang, P.; Wang, Z.; Wang, P.; Chishti, A. N.; Zhang, H.; Shi, J.; Ni, L.; Jamil, S.; Wei, Y. Supramolecular self-assembly of polyoxometalates and cyclodextrin: progress and perspectives. *Polyoxometalates* **2024**, *3*, 9140047.
(38) Wu, Y.; Shi, R.; Wu, Y.-L.; Holcroft, J. M.; Liu, Z.; Frasconi, M.; Wasielewski, M. R.; Li, H.; Stoddart, J. F. *J. Am. Chem. Soc.* **2015**, *137*, 4111−4118.
(39) Moussawi, M. A.; Leclerc-Laronze, N.; Floquet, S.; Abramov, P. A.; Sokolov, M. N.; Cordier, S.; Ponchel, A.; Monflier, E.; Bricout, H.; Landy, D.; Haouas, M.; Marrot, J.; Cadot, E. Polyoxometalate cationic cluster, and γ-cyclodextrin: from primary interactions to supramolecular hybrid materials. *J. Am. Chem. Soc.* **2017**, *139*, 12793−12803.
(40) Moussawi, M. A.; Haouas, M.; Floquet, S.; Shepard, W. E.; Abramov, P. A.; Sokolov, M. N.; Fedin, V. P.; Cordier, S.; Ponchel, A.; Monflier, E.; Marrot, J.; Cadot, E. Nonconventional three-component hierarchical host-guest assembly based on Mo-blue ring-shaped giant anion, γ-cyclodextrin, and Dawson-type polyoxometalate. *J. Am. Chem. Soc.* **2017**, *139*, 14376−14379.
(41) Guan, W.; Wang, G.; Li, B.; Wu, L. Organic macrocycle-polyoxometalate hybrids. *Coord. Chem. Rev.* **2023**, *481*, 215039.
(42) Falaise, C.; Moussawi, M. A.; Floquet, S.; Abramov, P. A.; Sokolov, M. N.; Haouas, M.; Cadot, E. Probing dynamic library of metal-oxo building blocks with γ-cyclodextrin. *J. Am. Chem. Soc.* **2018**, *140*, 11198−11201.
(43) Ni, L.; Li, H.; Xu, H.; Shen, C.; Liu, R.; Xie, J.; Zhang, F.; Chen, C.; Zhao, H.; Zuo, T.; Diao, G. Self-assembled supramolecular polyoxometalate hybrid architecture as a multifunctional oxidation catalyst. *ACS Appl. Mater. Interfaces* **2019**, *11*, 38708−38718.
(44) Yang, P.; Zhao, W.; Shkurenko, A.; Belmabkhout, Y.; Eddaoudi, M.; Dong, X.; Alshareef, H. N.; Khashab, N. M. Polyoxometalate-cyclodextrin metal-organic frameworks: from tunable structure to customized storage functionality. *J. Am. Chem. Soc.* **2019**, *141*, 1847−1851.
(45) Falaise, C.; Khlifi, S.; Bauduin, P.; Schmid, P.; Shepard, W.; Ivanov, A. A.; Sokolov, M. N.; Shestopalov, M. A.; Abramov, P. A.; Cordier, S.; Marrot, J.; Haouas, M.; Cadot, E. "Host in host" supramolecular core-shell type systems based on giant ring-shaped polyoxometalates. *Angew. Chem., Int. Ed.* **2021**, *60*, 14146−14153.
(46) Liu, X.; Zhang, J.; Lan, Y.; Zheng, Q.; Xuan, W. Infinite building blocks for directed self-assembly of a supramolecular polyoxometalate-cyclodextrin framework for multifunctional oxidative catalysis. *Inorg. Chem. Front.* **2022**, *9*, 6534−6543.
(47) Nie, S.-Q.; Yuan, Y.-Y.; Zeng, H.-M.; Jiang, Z.-G.; Zhan, C.-H. Homohelical self-assembly of trimer of α-cyclodextrin and octamolybdate. *Inorg. Chem.* **2023**, *62*, 19153−19158.
(48) Ni, L.; Gu, J.; Jiang, X.; Xu, H.; Wu, Z.; Wu, Y.; Liu, Y.; Xie, J.; Wei, Y.; Diao, G. Polyoxometalate-cyclodextrin-based cluster-organic supramolecular framework for polysulfide conversion and guest-host recognition in lithium-sulfur batteries. *Angew, Chem. Int. Ed.* **2023**, *62*, No. e202306528.
(49) Zhang, M.-M.; Yin, Y.-A.; Chen, W.-J.; Lin, C.-G.; Wei, Y.; Song, Y.-F. Asymmetric modification of Anderson-type polyoxometalates towards organic-inorganic homo- and hetero-cluster oligomers. *Inorg. Chem. Front.* **2023**, *10*, 1712−1720.
(50) Zhuang, Q.; Sun, Z.; Lin, C.-G.; Qi, B.; Song, Y.-F. Latest progress of asymmetrically functionalized Anderson-type polyoxometalates. *Inorg. Chem. Front.* **2023**, *10*, 1695−1711.
(51) Wu, P.; Wang, Y.; Huang, B.; Xiao, Z. Anderson-type polyoxometalates: from structures to functions. *Nanoscale* **2021**, *13*, 7119−7133.
(52) Zhang, J.; Long, Y.; Xuan, W.; Lin, C.-G.; Song, Y.-F. Preparation of polyoxometalate-chalcone hybrid and its photopolymerization property (in Chinese). *Chin. Sci. Bull.* **2017**, *62*, 685−692.
(53) Scelle, J.; Vervoitte, H.; Bouteiller, L.; Chamoreau, L.-M.; Sollogoub, M.; Vives, G.; Hasenknopf, B. Size-dependent compression of threaded alkyldiphosphate in head to head cyclodextrin [3]pseudorotaxanes. *Chem. Sci.* **2022**, *13*, 2218−2225.
(54) Akae, Y.; Koyama, Y.; Kuwata, S.; Takata, T. Cyclodextrin-based size-complementary [3]rotaxanes: selective synthesis and specific dissociation. *Chem.−Eur. J.* **2014**, *20*, 17132−17136.
(55) Blight, B. A.; Ahmad, T. I.; Shepherd, H. J.; Jennings, C. S.; Ferland, L. I.; Teat, S. J.; Rossman, J. S. Sterol uptake by an alkali-β-cyclodextrin metal-organic framework. *Cryst. Growth Des.* **2020**, *20*, 43−48.
(56) Niu, Y.; Jia, L.; Li, Y.; Liu, Y.; Yin, Q.; Zhou, L. Insights into structural features and ternary phase diagrams of prednisolone/β-cyclodextrin inclusion complex. *Cryst. Growth Des.* **2023**, *23*, 6431−6441.
(57) Schmidt, G. M. J. *Solid State Photochemistry*; Verlag Chemie: Weinheim, 1976.
(58) Fura, G. D.; Long, Y.; Yan, J.; Chen, W.; Lin, C.-G.; Song, Y.-F. Synthesis, structural characterization and fluorescence enhancement of chromophore-modified polyoxometalates. *Acta Cryst. C* **2018**, *74*, 1260−1266.
(59) Guan, W.; Wang, G.; Ding, J.; Li, B.; Wu, L. A. supramolecular approach of modified polyoxometalate polymerization and visualization of a single polymer chain. *Chem. Commun.* **2019**, *55*, 10788−10791.
(60) Kory, M. J.; Wörle, M.; Weber, T.; Payamyar, P.; van de Poll, S. W.; Dshemuchadse, J.; Trapp, N.; Schlüter, A. D. Gram-scale synthesis of two-dimensional polymer crystals and their structure analysis by X-ray diffraction. *Nat. Chem.* **2014**, *6*, 779−784.
(61) Chen, X.-Y.; Chen, H.; Đorđević, L.; Guo, Q.-H.; Wu, H.; Wang, Y.; Zhang, L.; Jiao, Y.; Cai, K.; Chen, H.; Stern, C. L.; Stupp, S. I.; Snurr, R. Q.; Shen, D.; Stoddart, J. F. Selective photodimerization in a cyclodextrin metal-organic framework. *J. Am. Chem. Soc.* **2021**, *143*, 9129−9139.

https://doi.org/10.1021/jacs.5c06495
J. Am. Chem. Soc. 2025, 147, 28903−28911